THE ASTROPHYSICAL JOURNAL, 441:L13–L16, 1995 March 1

HUBBLE SPACE TELESCOPE IMAGING OF A RADIO-QUIET GALAXY AT REDSHIFT $z = 3.4$[1,2]

MAURO GIAVALISCO, F. DUCCIO MACCHETTO,[3] PIERO MADAU, AND WILLIAM B. SPARKS
Space Telescope Science Institute, Baltimore, MD 21218
Received 1994 July 5; accepted 1994 December 8

ABSTRACT

We have observed with the Wide Field/Planetary Camera (WF/PC) on the *Hubble Space Telescope* (*HST*) a radio-quiet Lyα-emitting galaxy at redshift $z = 3.428$ (G2 below). The images probe the rest-frame UV light around 1250 Å with an angular resolution of $\approx 0\farcs1$, corresponding to 1.4 h_{50}^{-1} kpc at redshift $z = 3.4$ (in this *Letter* we use $q_0 = 0$ and $H_0 = 50\ h_{50}^{-1}$ km s^{-1} Mpc^{-1}). The light profile of the central $\sim 10\ h_{50}^{-1}$ kpc region is well fitted by an $r^{1/4}$ law with $r_e \approx 1.3\ h_{50}^{-1}$ kpc, suggesting a dynamically relaxed state. The outer regions are characterized by the presence of substructures, such as an elongated formation and low surface brightness nebulosities. The isophotal analysis shows no evidence of an AGN-like unresolved source in the center. The structural properties of G2 are consistent with a dynamically hot stellar system observed during an early phase of star formation, very likely the progenitor of an elliptical or the bulge of a spiral galaxy.

Subject headings: cosmology: observations — galaxies: distances and redshifts — galaxies: formation — galaxies: fundamental parameters — galaxies: starburst

1. INTRODUCTION

Despite many efforts to detect primeval galaxies, their general properties such as luminosity, spectral-energy distribution (SED), star-formation rate (SFR), and morphology remain still largely unknown (see Djorgovski 1992). High-redshift ($z > 2$) non–radio galaxy and cluster candidates have been identified in the past few years (Steidel & Hamilton 1992 and 1993, hereafter SH92 and SH93; Dressler et al. 1993; Giavalisco, Steidel, & Szalay 1994b, hereafter GSS; Hu & Ridgway 1994) and have been spectroscopically confirmed as such in some cases (Rowan-Robinson et al. 1991; Solomon, Radford, & Downes 1992; Lowenthal et al. 1991; Macchetto et al. 1993). However, the galaxies with measured redshift, typically due to their very high luminosity and/or a strong Lyα emission, seem to belong to a class of rather rare and unusual objects, and whether they are indeed the most extreme cases of a population of early starbursts or examples of a class of AGNs is still an open question.

The field around QSO Q0000−263 ($z_{QSO} = 4.11$) has received much attention over the last few years. Close to the QSO, SH92 have identified a galaxy whose impact parameter, apparent magnitude, and colors qualify it as responsible for the optically thick absorption system at $z_{abs} = 3.390$ observed in the QSO spectrum (hereafter galaxy A). At a separation of $\approx 87''$ from the QSO, Macchetto et al. (1993) have discovered a radio-quiet Lyα-emitting galaxy (hereafter G2) at $z = 3.428$ with identical colors to galaxy A (see also Giavalisco, Macchetto, & Sparks 1994a, hereafter GMS). Another 14 galaxies have been found with broad-band SED identical to A and G2 (SH93), with which they are spatially clustered to a confidence level of 98.8% (GSS), very likely forming a cluster of galaxies at redshift $z \sim 3.4$.

This association of galaxies has the potential to provide an insight into the physical conditions of protogalaxies in a cluster and, in particular, into an example of the long-sought high-redshift Lyα galaxies. Therefore, we have obtained WF/PC imaging of this field and report in this *Letter* about the morphology of galaxy G2 and address the key question whether its Lyα emission is really powered by the young, massive stars of a powerful starburst or whether the galaxy harbors a low-ionization, low-luminosity AGN.

2. THE DATA SET

The *HST* data consist of 4.7 hr of WFC integration through the filter F555W, similar to a *V* passband. Other scheduled observations through the F702W filter could not be carried out due to the failure of the solar array electronics that occurred in 1993 July. We complemented the *HST* data with CCD imaging in *V* and *R* from the ESO 3.5 m New Technology Telescope (NTT) in good seeing conditions ($0\farcs9$, with a scale of $0\farcs35$/pixel), totalling 60 and 40 minutes through the *V* and *R* filters, respectively.

We applied the Richardson-Lucy deconvolution algorithm (Lucy 1974; White 1990) to the *HST* images to correct for the effects of the spherical aberration. A well-exposed stellar image placed at about $22\farcs6$ (226 pixels) away from our main target was used as a point-spread function (PSF) for image restoration. We studied the PSF dependence on the CCD position using synthetic PSFs for the WF/PC created with the TINYTIM package (Krist 1994) and found that having used our star as a PSF did not significantly affect the results. We also studied the stability of the deconvolution algorithm on the number of iterations by reconvolving the restored images with the PSF, subtracting this blurred image model from the original frame, and studying the residuals. We found that the optimum number of iterations that minimizes these residuals for galaxy G2 is 28. We visually checked the reality of the morphological features in our fiducial deconvolved image to make sure that they were not coincident with any of the rings or tendrils of the PSF. Also, we checked that all the bright features present in the restored images were visible in the orig-

[1] Based on observations with the NASA/ESA *Hubble Space Telescope* obtained at the Space Telescope Science Institute which is operated by AURA under NASA contract NAS 5-26555.
[2] Based also on observations obtained at the European Southern Observatory, Las Silla, Chile.
[3] Affiliated with the Space Science Department, ESA.

inal frames as well, albeit as a much lower S/N. An offset, elongated structure that is evident in the deconvolved image was not clearly apparent in the raw image. However, this structure is detected in the NTT V image at the same position and orientation (feature "B," see Fig. 1 [Pl. L3]), strengthening the case for its reality. The *HST* image reaches a surface brightness of 28.54 mag/arcsec^2 at the 1 σ level.

The NTT images were debiased, flat-fielded, registered and co-added. We calibrated the fluxes using the standard LTT 1788 and LTT 9491 from the catalog by Stone & Baldwin (1983), deriving an error on the magnitude zero point of ≈ 0.03 mag for both passbands. The final V and R stacks reach a surface brightness of 27.85 and 27.63 mag/arcsec^2 at the 1 σ level, respectively.

3. MORPHOLOGICAL ANALYSIS

The new photometry of galaxy G2 is in very good agreement with previous measurements (see Table 1). Its morphology (see Fig. 1) is characterized by a bright, smooth central concentration (hereafter "core") surrounded by lower surface brightness nebulosities and a few compact substructures. To study the light profile we fitted elliptical isophotes to the deconvolved *HST* image and created a synthetic image that we have subtracted from the original to analyze the residuals. In principle, one should fit the center, ellipticity, and position angle of each individual isophote. However, the presence of the morphological disturbances and the relatively small numbers of pixels that form the image make this method inaccurate, as we have found from the analysis of the residuals. In particular, a major source of poor results was the fluctuations of isophote centers. We solved this by using the center derived from the inner isophote ($r < 0\farcs3$) with the smallest uncertainties, and keeping this center fixed, we selected the combination of ellipticities and position angles that minimized the residuals. In this way we produced our fiducial isophotal fit which has constant ellipticity and positional angle of $\epsilon = 0.11$ and P.A. = 144°, respectively.

Figure 2 shows the isophotal profile of galaxy G2. The error bars are the rms fluctuations of surface brightness along the elliptical path. Also plotted is the profile of a star scaled to the same magnitude and deconvolved with the same number of iterations as G2. It can be clearly seen in the figure that the

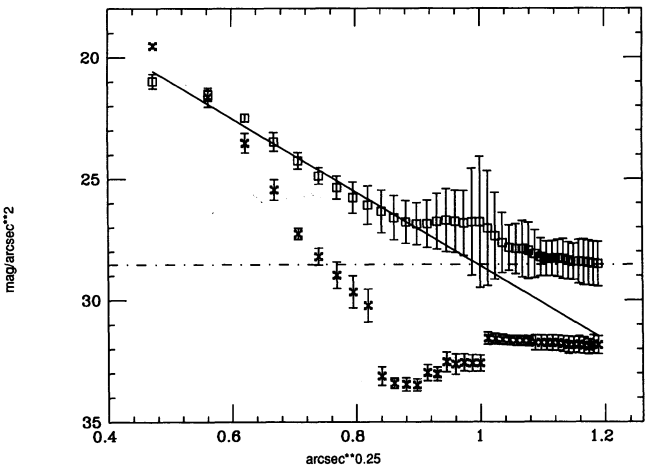

FIG. 2.—Plot of the light profile of galaxy G2 (*squares*), and, as a comparison, that of a star (*crosses*) scaled to the same magnitude and deconvolved with the same algorithm and number of iterations as G2. The continuous line represents an $r^{1/4}$ law. The horizontal dot-dashed line at $\mu = 28.54$ mag/arcsec^2 represents the 1 σ sky fluctuation of the image. Note that, while the adopted number of iterations is optimized for G2, it is not sufficient for a proper deconvolution of a stellar image. Therefore the real profile of a fully deconvolved star is actually sharper than the one in the diagram.

core of the galaxy is spatially extended. The inner region, namely $r \leq 0\farcs7$ or 9.8 h_{50}^{-1} kpc, is characterized by a smooth light profile that is well fitted by a de Vaucouleurs law with $r_e = (0\farcs09 \pm 0\farcs02)$ or $(1.3 \pm 0.3)\ h_{50}^{-1}$ kpc ($\chi_r^2 = 0.89$). An r^{-2} law produces a fit with much higher residuals ($\chi_r^2 = 1.8$). The dependence of the fitted value of r_e on the parameters of the adopted isophotal model is very weak, that is, the values of r_e fitted from models with different (but similar) ellipticity and position angle coincide within the errors. The apparent magnitude of the core, measured within a circular aperture of $1\farcs4$ diameter, is $V_{\rm core} = 24.0 \pm 0.1$. As shown in GMS, this number should be increased by ≈ 0.3 mag to obtain the magnitude of the continuum emission only, where the correction includes the contribution of the Lyα line and the dimming shortward of $\lambda_{\rm rest} = 1216$ Å due to intervening Lyα forest. This last, derived from the observed $G - \mathscr{R}$ color (SH93), is in excellent agreement with the theoretical expectation for an unreddened star-forming galaxy at $z \approx 3.4$ (Madau 1995).

TABLE 1

MEASURED PROPERTIES OF GALAXY G2

Band (1)	SH93 (2)	NTT (3)	*HST* (4)	μ (5)	σ (6)	r_e (7)
G	25.2 ± 0.2	...	...	...	415 ± 40	...
V	...	23.9 ± 0.2	24.0 ± 0.1	27.2	...	...
V, deconvolved	...	...	23.7 ± 0.1	26.9	...	1.3 ± 0.3
V, core	...	...	24.0 ± 0.1	24.5	...	$\chi_r^2 = 0.89$
V, "A"	...	...	27.3	27.1	...	...
V, "B"	...	26.7	26.7	25.7	...	...
V, "C"	...	...	27.7	26.4	...	...
R	...	24.1 ± 0.2	...	...	...	...
R, "B"		<27.0	...	...	...	...
$\mathscr{R}$	24.2 ± 0.2	...	...	...	...	...

NOTES.—Col. (2): Isophotal photometry in G and $\mathscr{R}$ (Steidel & Hamilton 1993). Magnitudes in the *AB* calibration. Col. (3): NTT isophotal photometry in V and R. The magnitudes of the features A, B, and C have been measured through polygonal apertures. Col. (4): *HST* V aperture photometry. The magnitude of the core is measured from the deconvolved image. Aperture diameters are 5″ for the whole galaxy and $1\farcs4$ for the core. Col. (5): *HST* V average surface brightness in the photometric aperture. Col. (6): Adopted value for the central velocity dispersion in km s^{-1} as calculated from the observed FWHM of the Lyα line. Col. (7): Effective radius of the core in h_{50}^{-1} kpc, fitted for $r < 0\farcs7$.

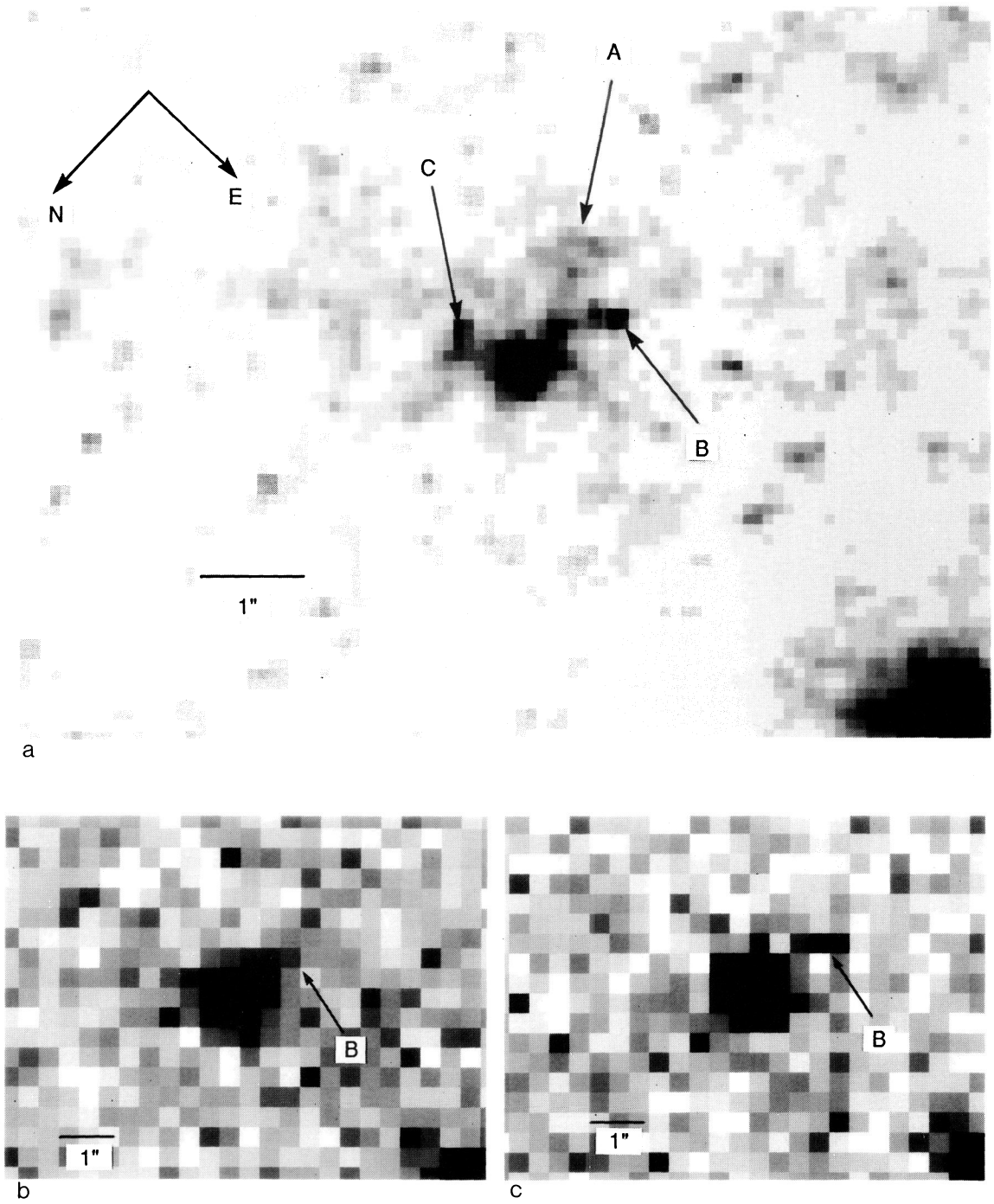

FIG. 1.—(*a*) A stack of 4.7 hr of WFC observations of galaxy G2 through the F555W passband. While the core of the galaxy has a smooth light profile, at larger radii morphological disturbances are observed as a diffuse nebulosity (feature A), an elongated, barlike structure (feature B), and a lump (feature C). An extended and diffuse nebulosity is also visible at larger distance from the center. (*b*) NTT stack of 40 minutes of integration in the *R* band. Same orientation as (*a*). (*c*) NTT stack of 1 hr of integration in the *V* band. Same orientation as (*a*). Note that the barlike formation "B" is detected in this frame (equivalent to the F555W), but not in the *R* frame, perhaps due to the fact that "B" is the site of Lyα emission.

For radial distances $r > 0''.7$, the $r^{1/4}$ law seems too steep to fit the isophotes. This could be due to the presence of a diffuse component ("halo" in the following), although the lower S/N in this region leaves open the possibility that this is actually an artifact of the deconvolution process. The average surface brightness profile of this region is better described by an r^{-2} law, while an exponential law results in higher rms residuals. Due to the large errors, however, a χ^2_r analysis cannot discriminate between these two profiles. This region is characterized by low surface brightness nebulosities and other more compact and brighter structures that result in an overall irregular morphology. They are clearly visible in Figure 2 as deviations from a regular light profile and highlighted by the large error bars, in contrast with the smoother profile of the inner core. We have defined polygonal apertures and measured the magnitude and average surface brightness of the most prominent of these structures (see Fig. 1*a* and Table 1), among which the elongated formation labeled "B" is interesting, as it is also detected in the NTT *V* frame.

The NTT *V* and *R* images of G2 are rather similar—note that the *R* band does not include the Lyα line— and both have angular size of $\sim 1''.1$ (after quadratic subtraction of the seeing profile), in agreement with the result from the *HST* image that the bright, inner part of the galaxy is indeed spatially resolved. The low surface brightness nebulosities present in the *HST* image are not detected in these frames. With the exception of structure "B," their average surface brightness is below the 3 σ level of the sky fluctuation. Considering also the effect of seeing, these faint structures are likely lost to the much higher sky luminosity. In the *V* frame, structure "B" is detected at $\approx 5\ \sigma$ level with an integrated magnitude $V = 26.7$ and an average surface brightness $\mu_V = 25.5$ mag/arcsec^2, in good agreement with the *HST* measurements. This formation is not detected in the *R* frame, and the corresponding 3 σ upper limits to its magnitude and average surface brightness in this passband are $R = 27.0$ and $\mu R = 26.5$ mag/arcsec^2. If its spectrum is similar to that of the core of the galaxy, then a dimming of ≈ 0.3 mag is expected when moving from the *V* to the *R* passband (GMS). Therefore, the measured limits are consistent with structure "B" having a flat UV continuum and a Lyα emission with equivalent width of ≈ 170–180 Å. Deeper imaging is necessary to further investigate this point.

4. DISCUSSION AND CONCLUSIONS

At $z = 3.4$ the Lyα from G2 has an observed equivalent width (relative to the continuum redward of the line) of $W\alpha = 775 \pm 70$ Å (GMS), contributing $\approx 45\%$ of the total observed *V* flux, or $\approx 80\%$ of the continuum flux. The isophotal analysis cannot exclude the presence of an unresolved AGN-like source in the center of the galaxy. If present, such a source could contribute up to $\approx 15\%$ of the observed flux (both continuum and line emission) and still be undetected as a deviation from the observed $r^{1/4}$ profile. It is highly unlikely, however, that the Lyα emission comes entirely from the inner $0''.1$ region, which contributes $\approx 50\%$ of the total *V* flux, because the continuum flux emitted from this region would be extremely small. Given the observed light profile, a more realistic possibility is that the observed light traces the stellar distribution, that is, line and continuum emission follow the same distribution, implying that stars and gas are well mixed on the scale of the angular resolution ($1.4\ h_{50}^{-1}$ kpc). In this case, due to the large Lyα equivalent width, no more than $\approx 25\%$ of the Lyα flux is emitted within the inner $0''.1$, and no AGN nucleus is necessary to explain the line emission. If only hot stars power the Lyα line, then its flux is very unlikely to exceed half of the continuum anywhere in the image, as the value of $W\alpha$ is already very close to the maximum predicted by stellar population synthesis models (Charlot & Fall 1993). In this case the fitted value of r_e should be largely independent from spatial variations in the line-to-continuum flux ratio. Future observations through a redder passband, such as the F702W, are clearly needed to clarify this point.

The observed properties of G2 suggest that this source is most likely a young galaxy undergoing a major episode of star formation. The inner light profile indicates that its core has reached the typical configuration of a dynamically hot (DH) galaxy, namely, one supported by its velocity dispersion. Models of the collapse of a protogalaxy, with (Silk & Norman 1981; Carlberg 1984; Carlberg, Lake, & Norman 1986; Baron & White 1987) and without (Van Albada 1982) dissipation, have shown that, due to the violent relaxation, a smooth equilibrium configuration forms within a few gravitational crossing times, whose light profile is well described by either an $r^{1/4}$ or an r^{-2} law. The intense star-formation activity of G2, with $SFR \approx 50$–$100\ h_{50}^{-1}\ M_\odot\ \mathrm{yr}^{-1}$ (GMS), would then be explained by the increased rate of dissipative cloud collisions as a consequence of the gravitational collapse (Silk & Norman 1981). We have further investigated this interpretation for G2 by comparing its properties with those of other DH systems observed at the present cosmological epoch. Specifically, we have derived its position relative to the "fundamental plane" (FP) of DH galaxies, for which we adopted the κ-space representation by Bender, Burnstein, & Faber (1992, hereafter BBF), where the three coordinates axes (κ_1, κ_2, κ_3) are linear combination of the logarithms of r_e, σ_0 (the central velocity dispersion), and $\mu_e(B)$ (the *B*-band mean surface brightness within r_e). If the core of G2 is a DH system undergoing a major star-forming phase, it would differ from its present-day counterparts primarily by having a high surface brightness and low M/L ratio. This implies that its representative point in the κ-space must have a small κ_3 value, as this largely depends on M/L, a large κ_2 value, which is dominated by the surface brightness (BBF), and must fall well below the FP.

We have calculated the position of G2 in the κ-space under the following assumptions: (1) the observed Lyα width of ~ 1000 km s^{-1} is mostly due to the central velocity dispersion of the stellar component, which yields $\sigma_0 \approx 400$ km s^{-1}, and (2) stellar population synthesis can be used to estimate the surface brightness in the rest-frame *B* band from the UV photometry, assuming an exponentially decaying burst with an *e*-folding time $\tau \sim 1$ Gyr observed at an age $T_* \approx 10^8$ yr (such a model, followed by a passive phase lasting ~ 14 Gyr, successfully explains the present SED of early-type galaxies; see, e.g., Bruzual & Charlot 1993). A burst as young as $\sim 10^8$ yr is consistent with the presence of Lya emission with large equivalent width, requiring a dust-free ISM (Charlot & Fall 1991) and a small filling factor of supernova remnants (Bithell 1991), and is comparable with the core crossing time $t_{\mathrm{cross}} \approx D_{\mathrm{core}}/\sigma_0 = 5 \times 10^7$ yr, where $D_{\mathrm{core}} = 20$ kpc. Under these assumptions, we find that at the epoch of observation G2 had absolute magnitude $B \approx -22.7$, or $L_B \approx 6L^*$ (adopting $M_B^* = -20.7$), which corresponds to an effective surface brightness $\mu_e(B) = 16.3$ mag/arcsec^2, after correcting for the $(1 + z)^4$ factor. Therefore, in the κ-space G2 has coordinates $\kappa_1 = 3.8$, $\kappa_2 = 5.6$, and $\kappa_3 = 0.48$. From Figure 2 of BBF, it can be seen that, as expected, *G2 lies indeed below the FP*, in particular below the

borderline region between ellipticals and bulges. This result remains valid even if a fraction as large as $\sim 50\%$ of the Lyα width is due to mechanisms other than the central velocity dispersion, such as resonant scattering, the velocity field of supernova shells, stellar winds, and rotational velocity. This is due to the fact that varying the velocity dispersion moves the galaxy in a direction that is almost parallel to the FP, while the shift along a direction perpendicular to it is largely controlled by the surface brightness.

Uncertainties on $\mu_e(B)$ depend on the evolutionary history of the galaxy. In the assumed model, the observed color $(G - \mathscr{R}) = 1.0 \pm 0.3$ (SH93), once dereddened by ≈ 0.6–0.8 mag due to Lyα forest absorption along the line of sight (Madau 1995), is consistent with an age $10^8 < T_* < 10^9$ yr, corresponding, in the limit of a transparent universe, to a color $0.1 < (G - \mathscr{R}) \lesssim 1$. If the galaxy is younger than 10^8 yr, the B luminosity is smaller, by about 60% or 0.5 mag if $T_* \sim 10^7$ yr. However, this is unlikely given the observed light profile and the core crossing time. The B luminosity is larger for an older galaxy, by about 0.5 mag for $T_* = \tau$. This would move the G2 point in the κ-space by $-0.08\,\kappa_3$ units and by $+0.12\,\kappa_2$ units, shifting it further away from the FP without significantly changing the predictions about the present-day luminosity. Therefore, as far as the deviation of G2 from the FP is concerned, our model age is actually a conservative choice. However, it seems rather unlikely that $T_* > \tau$, as the predicted unextincted $(G - \mathscr{R})$ color would be very red in this case, for example, $(G - \mathscr{R}) = 2.5$ for $T_* = 1.3\tau$.

An estimate of the mass in stars for G2 at the epoch of observation is $M_*(z = 3.4) \approx SFR \times T_* = 5 \times 10^9$–$10^{10}\ M_\odot$, suggesting that this object is the progenitor of a bright galaxy. Indeed, if the star-formation history of the core of G2 has given rise at $z = 0$ to the SED of an early-type galaxy, the corresponding luminosity evolution results in a surface brightness which is within the observed range for present-day ellipticals and bulges, and for which we estimate $20 \lesssim \mu_e(B) \lesssim 22$ mag/arcsec^2, depending on the evolution of r_e as M_* increases (we considered the cases of $r_e = \text{const}$ and $r_e \propto M_*^{1/3}$, which bracket all the possible cases if the core stellar density is not a decreasing function of M_*). The corresponding stellar mass would be $M_*(z = 0) \approx SFR \times \tau = 5 \times 10^{10}$–$10^{11}\ M_\odot$.

The possible presence at larger radii of a halo with an irregular morphology is consistent with the dissipative collapse (Baron & White 1987) of preexisting clouds characterized by a low SFR. In such a scenario a core-halo segregation is actually expected due to the increased cloud collision rate and SFR in the denser, more collapsed regions (Silk & Norman 1981). We note that the observed light distribution in this region supports this interpretation. Structures such as "A" and "B" could be isolated H II regions formed by a locally higher cloud collision rate and/or shock fronts from supernova explosions.

In conclusion, G2 appears to be a very young but otherwise normal galaxy, likely the progenitor of either a bulge or of an intermediate luminosity elliptical galaxy. This is consistent with the idea that in a cluster environment the larger ellipticals form by merging of smaller systems (BBF) and offers for the first time observational evidence that the dissipative collapse is a mechanism by which intermediate-size DH systems, either ellipticals or bulges, are formed, and we may be witnessing just such a process in action.

This research was supported by NASA through grant GO-4599.01-92A, awarded by the Space Telescope Science Institute, operated by AURA under contract NAS 5-26555.

REFERENCES

Baron, E., & White, S. D. M. 1987, ApJ, 322, 585
Bender, R., Burnstein, D., & Faber, S. M. 1992, ApJ, 399, 462 (BBF)
Bithell, M. 1991, MNRAS, 253, 320
Bruzual, G., & Charlot, S. 1993, ApJ, 405, 538
Carlberg, R. C. 1984, ApJ, 286, 403
Carlberg, R. C., Lake, G., & Norman, C. 1986, ApJ, 300, L1
Charlot, S., & Fall, S. M. 1991, ApJ, 378, 471
———. 1993, ApJ, 415, 580
Djorgovski, S. 1992, in Cosmology and Large Scale Structure in the Universe, ed. R. R. de Carvalho (ASP Conf. Series 24), 73
Dressler, A., et al. 1993, ApJ, 404, L45
Giavalisco, M., Macchetto, D. F., & Sparks, W. B. 1994a, A&A, 288, 103 (GMS)
Giavalisco, M., Steidel, C. C., & Szalay, A. S. 1994b, ApJ, 425, L5
Hu, E. M., & Ridgway, S. E. 1994, AJ, 107, 1303
Krist, J. 1994, TINYTIM User's Manual, version 2.3
Lowenthal, J. D., et al. 1991, ApJ, 377, L73
Lucy, L. B. 1974, AJ, 79, 745
Madau, P. 1995, ApJ, 441, 18
Macchetto, F. D., et al. 1993, ApJ, 404, 511
Rowan-Robinson, M., et al. 1991, Nature, 351, 719
Silk, J., & Norman, C. 1981, ApJ, 247, 59
Solomon, P. M., Radford, S. J. E., & Downes, D. 1992, Nature, 356, 318
Steidel, C. C., & Hamilton, D. 1992, AJ, 104, 941 (SH92)
———. 1993, AJ, 105, 2017 (SH93)
Stone, R. P., & Baldwin, J. A. 1983, MNRAS, 204, 357
Van Albada, T. S. 1982, MNRAS, 201, 939
White, R. L. 1990, in The Restoration of HST Images and Spectra, ed. R. L. White & R. J. Allen (Baltimore: STScI), 139